Journal of Membrane Science 596 (2020) 117606

Contents lists available at ScienceDirect

Journal of Membrane Science

journal homepage: http://www.elsevier.com/locate/memsci

The prediction of the operating conditions on the permeate flux and on protein aggregation during membrane processing of monoclonal antibodies

Lara Fernandez-Cerezo [a,b], Andrea C.M.E. Rayat [a,*], Alex Chatel [a], Jennifer M. Pollard [b], Gary J. Lye [a], Mike Hoare [a]

[a] The Advanced Centre for Biochemical Engineering, Department of Biochemical Engineering, UCL, Gower St, London, WC1E 6BT, UK
[b] Downstream Process Engineering and Development, Merck & Co., Inc, 2000 Galloping Hill Road, Kenilworth, NJ, 07033, USA

ARTICLE INFO

Keywords:
Tangential flow filtration
Ultra scale-down
Ultrafiltration/diafiltration
High monoclonal antibody concentration
Protein aggregation

ABSTRACT

The lack of available material during early stage bioprocess development poses numerous processing challenges such as limiting the number of full-scale experiments. Extended fundamental process understanding could be gained with the use of an ultra scale-down (USD) device using as little as 1.7 mL per experimental run. The USD system is used to predict diafiltration and ultrafiltration/diafiltration (UF/DF) performance of a pilot-scale tangential flow filtration (TFF) system, fitted with a flat-sheet cassette, operating at 500-fold larger scale. Both systems were designed by maintaining a volumetric loading of 8.1 L of feed per m^2. Permeate flux was predicted for monoclonal antibody solutions with the USD system across a range of transmembrane pressure drops, feed concentrations and flow conditions during diafiltration, and desired retentate concentrations during UF/DF operations. The resulting USD data were in good agreement with the pilot-scale TFF when scaled based on similar shear rates over the membrane surface. Little change in soluble aggregates was observed in both systems but there were significantly higher increases in product turbidity in the USD system. A correlation was established to relate turbidity increase based on the volume fraction of high shear stress zone for USD systems and various pilot-scale TFF systems. The correlation was extended to encompass the processing time and concentration for a wide range of membrane processing challenges in both scales.

1. Introduction

Membrane processes are integral to industrial processes including monoclonal antibody downstream operations where microfiltration, ultrafiltration and viral filtration membranes are increasingly applied [1,2]. One use of ultrafiltration membranes in these operations is for product concentration and for an exchange to, for example, a formulation buffer [3,4]. These concentration and buffer exchange operations are often simply referred to as ultrafiltration/diafiltration (UF/DF) in the biopharmaceutical industries. The main objectives of UF/DF steps are volume reduction (UF) and buffer exchange of the incoming solution (DF), respectively. This paper demonstrates the application of a rotating disc ultra scale-down (USD) membrane system to predict how a tangential flow filtration (TFF) system performs at pilot-scale using an ultrafiltration membrane in a flat-sheet cassette format.

Membrane processes using flat-sheet cassettes are often scaled by changing the number of cassettes or membrane sheets (i.e. to alter the membrane area) while maintaining the same transmembrane pressure, crossflow rate, membrane loading and functional design (i.e. flow path length) [5,6]. Membrane loading is defined by the total feed volume, or mass, to be processed per m^2 of membrane area in the initial concentration stage. Loadings range from 200 to 1000 g of protein per m^2 (typically 25–120 L of protein solution per m^2) with an average of 450 g/m^2 [4]. A trade-off exists between a target membrane loading, total membrane area requirement, and total processing time. For example, when processing a shear- sensitive product, a lower loading may be targeted to result in a reduced duration by using a larger membrane area. Where reducing the membrane area is a priority, a higher loading will be targeted by using longer process times. The relationship among these different parameters are shown in Equation (1)–(2).

* Corresponding author.
E-mail address: Andrea.rayat@ucl.ac.uk (A.C.M.E. Rayat).

https://doi.org/10.1016/j.memsci.2019.117606
Received 12 June 2019; Received in revised form 30 September 2019; Accepted 23 October 2019
Available online 30 October 2019

$$Membrane\ loading\ \left(g\ /\ m^2\right) = \frac{Total\ feed\ volume\ to\ be\ processed\ (L)\ x\ Feed\ concentration\ (mg/mL)}{Total\ membrane\ area\ (m^2)} \quad (1)$$

$$Total\ membrane\ area\ \left(m^2\right) = \frac{Permeate\ volume\ (L)}{Total\ duration\ (h)\ x\ Permeate\ flux\ (L/m^2/h)} \quad (2)$$

Additionally, the use of membrane loadings allows the design to account for a range of incoming feed concentrations to an UF/DF step. For example, UF/DF steps in monoclonal antibody processing often follow polishing chromatographic steps [2]. These steps will yield different product concentrations. A flow-through anion exchange (AEX) chromatography will yield a dilute process stream while a bind-and-elute cation exchange (CEX) chromatography step often delivers a more concentrated stream. This means that for the same target membrane loading, a larger volume of feed stream will be processed from a flow-through AEX chromatography than from a bind-and-elute CEX chromatography step. Since the available membrane area in biomanufacturing facilities is often fixed, this has implications on operational costs (for an oversized membrane area) or processing time (for an undersized membrane area) and consequently, on the stability of the product.

A challenge is to determine the membrane loadings needed ahead of full-scale trials to help decide the appropriate total membrane area requirements at large-scale. Recent efforts have focused on the development of an ultra scale-down (USD) device (at least 1.7 mL working volume) to predict operations at pilot-scale, which for a previous study required a working volume of ~890 mL per experiment [7]. The USD device uses the rotation of a disc to allow decoupling of the dependencies between the flow over the membrane surface and the transmembrane pressure or flux. More specifically, implementation of this device to predict the flux of a pilot-scale TFF system as a function of shear rate during monoclonal antibody diafiltration experiments was demonstrated by our previous work [7].

The prediction of the effect of membrane bioprocessing on product quality attributes, such as dimer content and product variants, is also key to successful scale-down. UF/DF operations are often among the final bioprocess unit operations beyond which there are few or even no further purification stages except bioburden reduction during bulk filtration [1,2,8,9]. These operations can take place in different combinations, i.e. stand-alone UF or DF, or a combined UF/DF, depending on the individual location within the bioprocess sequence. For example, the final step prior to bioburden reduction typically takes place as UF/DF/UF where the incoming feed is initially concentrated, followed by buffer exchange to the formulation buffer, and then further concentrates to reach the target protein concentration. If the UF/DF step takes place between different chromatographic steps or a lower protein concentration is targeted, it can run as UF/DF with no further ultrafiltration step. It is important to control product quality, e.g. dimer content, particularly for unstable proteins where a small change in aggregate levels may have a significant impact on efficacy and safety considerations [10]. Protein aggregates can be categorised in many ways including whether they are reversible or irreversible, soluble or insoluble, or by size [11]. It is thought that small soluble reversible oligomers are first formed by protein binding at charged or polarised regions [12,13]. These trigger the formation of partially folded protein intermediates, which are known to be precursors to small oligomers [14,15]. The latter may begin to associate through irreversible bonding, and eventually become covalently-bonded insoluble aggregates through, for example, the formation of disulphide bonds through intermolecular thiol linkage [16–18]. These aggregates may become large, often visible, and removable using a 0.22 μm filter [19].

During UF/DF stages, proteins are exposed to high shear stress environments and shear-associated conditions including: multiple pump and valve passes per cycle; air-bubble entrainment [20]; adsorption to stainless steel [21]; solid-liquid interfacial effects [22,23]; and shear-related pump microactivation [24]. Proteins are also exposed intermittently to membrane surfaces, where a high concentration gel layer may form possibly triggering the formation of aggregates [25–27]. The choice of pump is additionally known to affect stability; for example, the use of peristaltic [28] and screw pumps [29] tend to cause higher aggregate levels possibly due to increased back pressure and thus, increasing pump "shear" [30].

This paper will focus on predicting the membrane performance across a range of transmembrane pressures, flow conditions (represented by shear rate), feed and retentate concentrations during ultrafiltration and diafiltration operations. This will include a comparison of the dimer content of the resulting solutions as measured by size exclusion chromatography and turbidity to track aggregate formation.

2. Materials and methods

System components and the experimental method followed are fully detailed elsewhere [7]. For convenience, salient details are provided below.

2.1. Materials

Humanized monoclonal antibodies mAb-A (~150 kDa, pI 9.0) and mAb-B (~150 kDa, pI 7.6), were provided by Merck Sharp & Dohme Corp., a subsidiary of Merck & Co., Inc., Kenilworth, NJ, USA as ~ 12 mg/mL solutions in 10 mM Sodium Acetate, pH 5.5, −80°C. These were thawed overnight, concentrated to 30 mg/mL (mAb-A) and 155 mg/mL (mAb-B) followed by buffer exchange into 10 mM Tris Acetate pH 5.4 using the same method, membrane type and equipment as described below and in Ref. [7]. The resultant solutions were diluted using the latter buffer as required. These were used within 24 h.

Buffer materials were obtained from Sigma-Aldrich (St. Louis, MO). Buffer solutions were pre-filtered with sterilising filter (Steritop bottle-top filters, 0.22 μm pore size, EMD Millipore, Bedford, MA).

2.2. Equipment and experimental methods

2.2.1. Pilot-scale and lab-scale TFF systems and experiments (see Ref. [7])

The main pilot-scale system used is described in Ref. [7] (Pendo-TECH TFF Process Control™ rig fitted with a quaternary diaphragm pump (QuattroFlow™ 150 S, Triangle Process Equipment, Wilson, NC) and a 0.11 m^2 membrane cassette (MWCO 30 kDa, composite regenerated cellulose, C-screen Pellicon 3, EMD Millipore, Bedford, MA)). For one experiment, a rotary lobe pump (200–576, UNIBLOC®-PD, Unibloc-Pump, Inc, Marietta, GA) was used. The working volume for this system was usually 890 mL, unless otherwise stated. The laboratory-scale TFF system operated using a diaphragm pump (XX42PMP01, Lab-scale pump module TFF system, EMD Millipore, MA) and was fitted with a 0.005 m^2 membrane cassette (same specification as above) with a working volume of ~50 mL.

All trials were performed at constant mean transmembrane pressure drop, $\Delta\overline{P}_{TMP}$, of typically 1 bar. Constant $\Delta\overline{P}_{TMP}$ was attained using retentate valve control in both TFF systems; automatic in the pilot-scale while manual in the lab-scale. The trials were conducted at room temperature (~20 °C).

Six main stages for the TFF studies were performed: (1) system set-up (drain and install new cassette); (2) system equilibration (wash with water to measure membrane resistance and then with diafiltration buffer); (3) manual loading; (4) fed-batch diafiltration or two-stage ultrafiltration/diafiltration (feed or diafiltration buffer controlled to match the permeate flux); (5) product collection; (6) system clean and storage at room temperature (with 0.1 N NaOH).

2.2.2. USD system and experiments

The USD device comprises a 1.7 mL Perspex chamber (Ø = 25 mm (inner diameter, (ID)), h = 56 mm) and a support frit in the stainless-steel base to hold the membrane disc in place (Ø = 25 mm, with the same membrane material as the TFF system). An alternative 6.3 mL Perspex chamber (Ø = 25 mm (ID), h = 193 mm) was also used. For both chambers, the stainless-steel rotating disc is located 2.0 mm above the membrane surface. The active membrane is presented as a concentric ring; 2.1 cm^2 area, ID = 8 mm and OD = 18 mm. For a schematic diagram of the USD device, see Ref. [7]. The device contents were maintained at a fixed temperature (20 °C) and at constant pressure (1 bar, unless otherwise specified) by controlling the syringe pump flowrate.

Six main stages were performed for the USD studies: (1) system set-up (with new pre-wetted filter disc); (2) system equilibration (wash with water to measure membrane resistance, and then with diafiltration buffer); (3) manual load of antibody solution; (4) fed-batch diafiltration or two-stage ultrafiltration/diafiltration (by automatic feeding at the desired ΔP_{TMP}); (5) manual product collection; and (6) system clean and storage at room temperature (0.1 N NaOH).

Two different types of pilot-scale TFF and USD experiments, diafiltration and ultrafiltration, were conducted in fed-batch configuration (i.e. constant retentate volume), as shown in Fig. 1. For diafiltration experiments, firstly steady-state flux rate as a function of transmembrane pressure drop characteristic profile for increasing pressure drop up to 1.6 bar was measured. This characteristic profile was recorded for

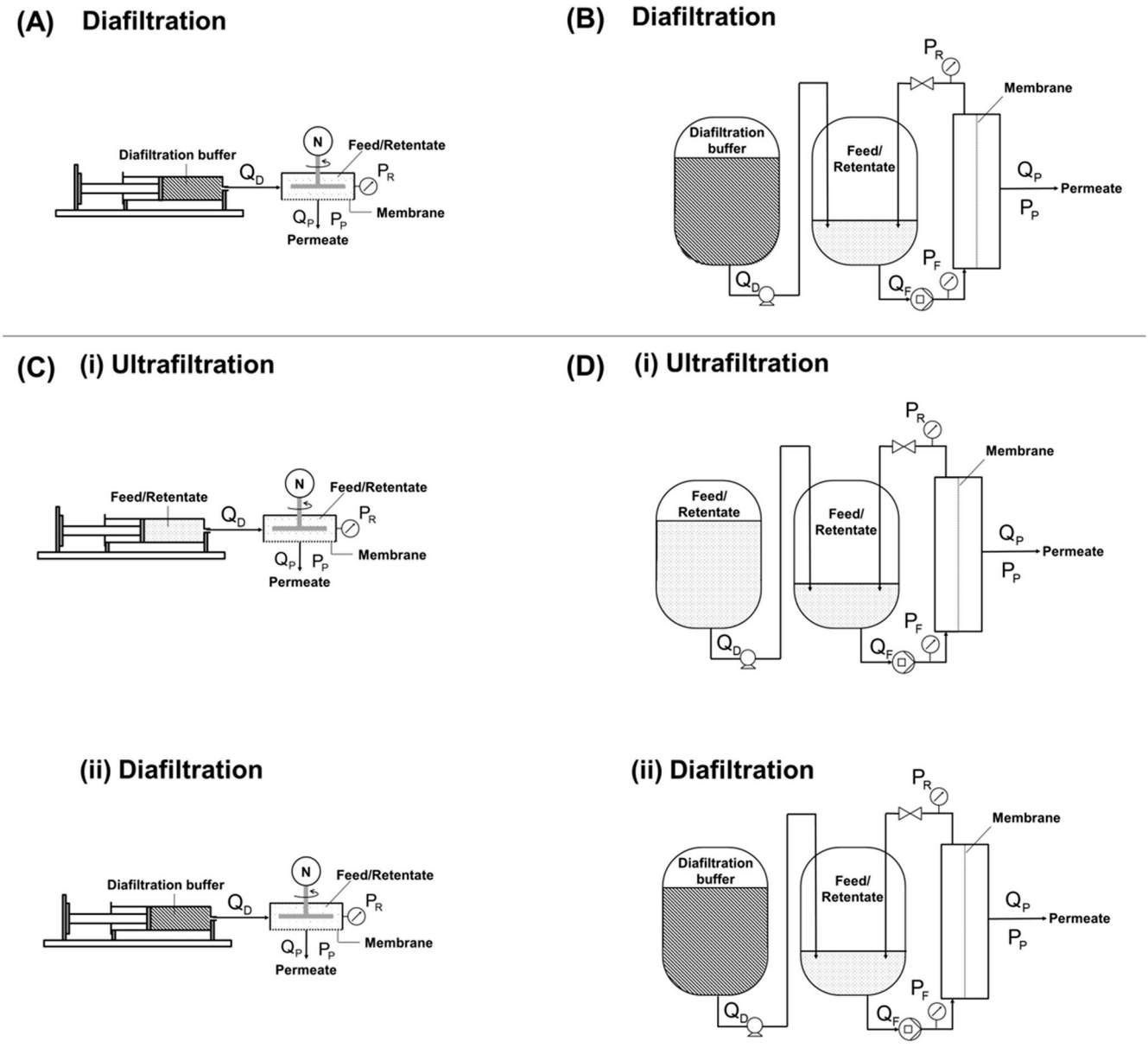

Fig. 1. Schematic representation for fed-batch diafiltration operation of the (A) ultra scale-down (USD) and (B) lab-scale TFF and pilot-scale TFF membrane systems; and two-stage fed-batch ultrafiltration/diafiltration operation of the (C) ultra scale-down (USD) and (D) pilot-scale TFF membrane systems. In this paper the membrane areas are 0.00021 m^2 for the USD system, 0.005 m^2 for the lab-scale TFF system and 0.11 m^2 for the pilot-scale TFF system. The volume of protein feed per membrane area is maintained the same. Note that the drawings are not drawn to scale.

combinations of a protein solution concentration and a flow condition over the membrane at equivalent shear rates for USD and TFF scales (Details on shear rate calculations are given in Ref. [7]). A second type of diafiltration experiment was conducted where the transient flux rate versus time profile was measured across a range of protein solution concentrations at a single transmembrane pressure drop (1.0 bar) and single flow condition over the membrane during a 7 diafiltration volume (DV) operation. For all ultrafiltration experiments the transient flux rate versus time profile were also measured for a fixed initial protein concentration (12 mg/mL) at a single flow condition (i.e. the same average shear rate over the membrane) and for combinations of the final protein solution concentration. A new membrane was used for each diafiltration run or combination of ultrafiltration and diafiltration runs.

2.3. Analyses

A capillary viscometer (m-VROC, RheoSense ©, San Ramon, CA) was used to measure the viscosity of the diafiltration buffer and the feed solutions (1–155 mg/mL).

Soluble protein aggregates were quantified using size-exclusion chromatography (UP-SEC using YMC Pack-Diol 120 column, 5 µm, 8 × 300 mm, YMC, Kyoto, Japan operated using an Agilent 1200 Chemstation Agilent Technologies, US). The injection volume of each sample was adjusted to target a mass of 5 µg. The method used a flowrate of 0.5 mL/min and a 214 nm UV detection wavelength.

Turbidity was recorded using optical density (OD) at 650 nm (SpectraMax Plus® 384 Microplate Reader, Molecular Devices LLC, San Jose, CA).

3. Results and discussion

3.1. Experimental design

The performances of the USD and the pilot-scale TFF systems were compared in two different modes: fed-batch diafiltration (DF) (Fig. 1A and B) and two-stage fed-batch ultrafiltration followed by diafiltration (terminology used here is ultrafiltration/diafiltration, UF/DF) (Fig. 1C and D). The lab-scale TFF system was only operated in fed-batch diafiltration operation (Fig. 1B).

The systems were scaled at a constant volumetric membrane loading of 8.1 L of feed per m^2. This for example is equivalent to a mass loading of 97 g/m^2 for a 12 mg/mL feed solution. The flow conditions in both systems were kept comparable in terms of the average shear rate (studied range from ~2000 to ~7000 s^{-1}) within a 0.1 mm-height of fluid above the membrane surface (i.e. half the effective channel height, between two membranes in flat-sheet cassettes [4]). For the USD system, the shear rates were obtained using computational fluid dynamics and for the TFF system using pressure drop-flowrate characteristic profile as described elsewhere [7]. The rheology for the two monoclonal antibody solutions studied is considered to be Newtonian across the explored range of concentrations and shear rates ($n = 1.01 \pm 0.02$ for $\mu = k\,\bar{\gamma}_{av}^{n-1}$) (Fig. 2A). The resulting correlation between viscosity, µ, and feed concentration, C ($\mu = 1.01\ e^{0.017C}$) (Fig. 2B) is similar to that reported elsewhere [31].

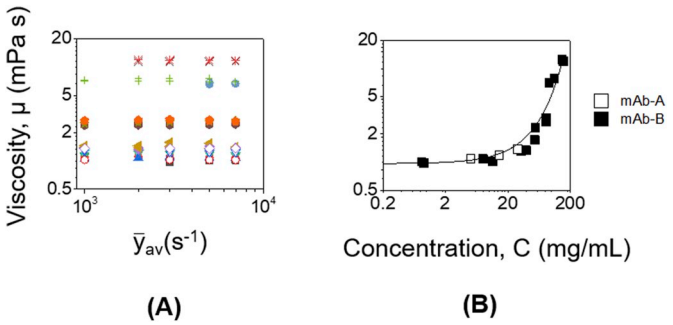

Fig. 2. Effect of the viscosity of mAb-A and mAb-B solutions (A) as a function of average shear rate, $\bar{\gamma}_{av}$ and (B) as a function of concentration at a fixed $\bar{\gamma}_{av} = 2200\ s^{-1}$. In (A), the chosen range (1000–7000 s^{-1}) was representative of the flow conditions for typical crossflow rates in flat-sheet membrane cassettes [7]. Here, mAb-A values are shown by open data points, while mAb-B are closed. Coefficient values of $n = 1.01 \pm 0.02$ ($\mu = k\,\bar{\gamma}_{av}^{n\,-1}$) were obtained for all concentrations studied (0.7–155 mg/mL). In (B), an exponential trend has been fitted using $\mu = Ae^{BC}$ (where C is concentration (mg/mL), and A = 1.01 mPa·s and B = 0.017 mL/mg) with $R^2 = 0.95$. The different concentrations were made as dilutions from a stock solution of 30 mg/mL for mAb-A and 155 mg/mL for mAb-B. Viscosity was measured at a controlled temperature of 20.00 ± 0.05 °C in triplicate (error bars (±1 s d.) lie within the data points).

3.2. Factors affecting the experimental design space during diafiltration

A series of USD experiments in diafiltration mode (Fig. 1A) and pilot-scale TFF (Fig. 1B) were performed to measure the steady-state flux at increasing transmembrane pressure drop for three feed concentrations of mAb-A at four disc speeds (USD, Fig. 3i) and four crossflow rates (TFF, Fig. 3ii). Diafiltration mode was selected using the same composition for the diafiltration buffer as that in the feed solution to maintain a constant ionic environment. This enabled an assessment of the diafiltration performance as a function of feed and operating conditions only without the additional effect of change in ionic environment. The flow conditions were characterised based on an average shear rate ($\bar{\gamma}_{av}$) which is achieved by a specific rotational speed (N, in rpm) of the USD system (Fig. 3iii) and/or crossflow rate (Q_F, in L/min/m^2 (LMM)) of the pilot-scale TFF system (Fig. 3iv).

A transition from pressure-dependent to pressure-independent flux was observed for all conditions tested in the USD (Fig. 3i) and in the pilot-scale TFF (Fig. 3ii) systems with decreasing flux as the feed concentration is increased and increasing flux as the crossflow rate is increased. The transmembrane pressure ($\Delta\bar{P}_{TMP} = \frac{P_F + P_R}{2} - P_P$)at which the transition occurs depends on the shear rate and concentration. It was observed to occur at a similar combination of conditions in both scales (Fig. 3i–3ii). For example, at a 5 mg/mL feed concentration and a shear rate of 2400 s^{-1} (N = 2100 rpm, Q = 4 LMM) it is observed to occur at a ΔP_{TMP} of 0.9-1.0 bar at both scales (Fig. 3Ai and 3Aii).

In Fig. 3i and 3ii, an exponential curve was fitted to each of the data. Each curve represents a single experiment (n = 1) for both systems. Previous work has shown that replicate runs using the USD system has a coefficient of variation (CoV) of less than 5%. To create the exponential curves, an empirical correlation, $J = a\,(1 - b^{\Delta P_{TMP}})$, was selected based on the criterion that the correlation should demonstrate typical relationship between J and ΔP_{TMP}, as extensively reported in literature, e.g. in literature [32], with the assumption that the model had to go through (0,0) and have a limiting maximum value. This empirical correlation has the properties of $J = 0$, $\Delta P_{TMP} = 0$ and J approaches a maximum limiting value (equal to *a*) for increasing ΔP_{TMP}, i.e. $b < 1$. For all data sets the expected trends are observed and good fits were obtained ($R^2 > 0.99$). Similar quality fits were observed for the pilot-scale TFF data ($R^2 > 0.98$).

Direct matching in terms of the permeate flux of the USD and pilot-scale TFF correlations is not attempted here due to the slightly different flow conditions. However, similar results are observed for both systems but with noticeably higher values of J at low ΔP_{TMP} for the USD device. The profiles at the lowest flow conditions also tended to be of higher flux rates for the USD device. These differences will be further explained following a more detailed analysis of the parity between USD and TFF data.

To aid this analysis, a design space (Fig. 4i) to evaluate the effects of ΔP_{TMP} and $\bar{\gamma}_{av}$ was developed from the USD flux data (Fig. 3i). This was performed by combining the results from the four J vs. ΔP_{TMP} correlations for each flow condition and generating a data matrix for the

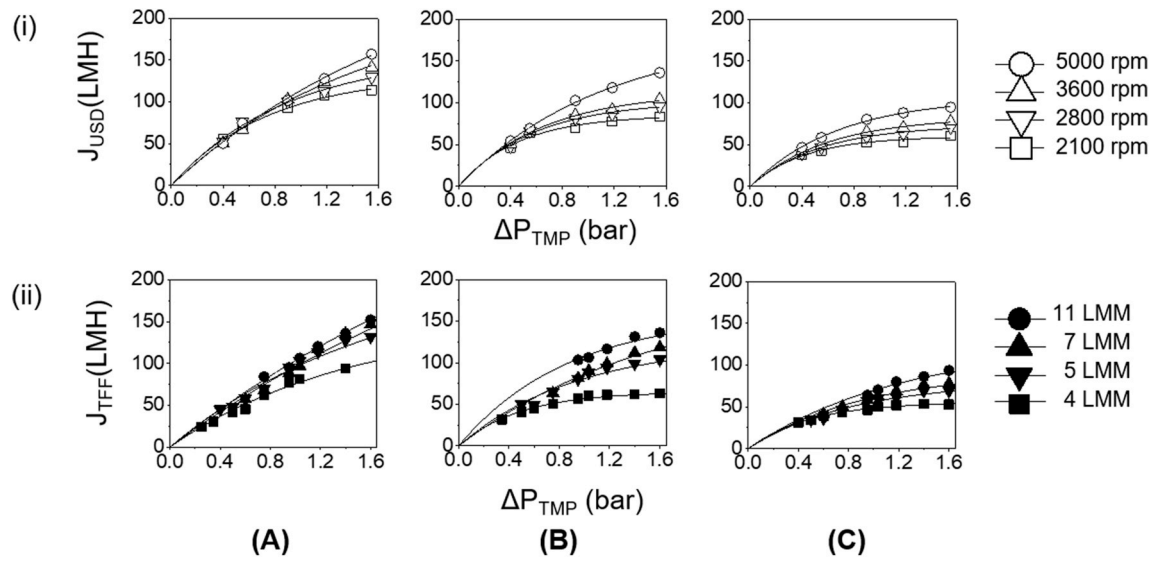

(iii)

N (rpm)	$\bar{\gamma}_{av}$ (s^{-1}) 5 mg/mL 0.00103 Pa s	15 mg/mL 0.00120 Pa s	30 mg/mL 0.00137 Pa s
2100	2400	2300	2100
2800	3600	3400	3300
3600	5000	4800	4600
5000	7400	7300	7100

(iv)

Q_F (LMM)	$\bar{\gamma}_{av}$ (s^{-1}) 5 mg/mL 0.00103 Pa s	15 mg/mL 0.00120 Pa s	30 mg/mL 0.00137 Pa s
4	2400	2200	2100
5	3700	3500	3300
7	5000	4900	4600
11	7600	7300	6800

Fig. 3. Effect of flow conditions on flux - transmembrane pressure drop profiles for the USD and the pilot-scale TFF systems.
The three concentrations of mAb-A used in these experiments were: (A) 5 mg/mL, (B) 15 mg/mL, and (C) 30 mg/mL. In (i) and (ii), fitted exponential curves ($J = a(1 - b^{\Delta P_{TMP}})$) are shown where a, b are constants unique to each experimental condition ($R^2 = 0.999$). In (iii), the corresponding average shear rates from CFD simulations are shown for each concentration and disc speed used for the USD system. In (iv), the average shear rates are shown for each concentration and crossflow rate assume non-laminar conditions for the pilot-scale TFF runs. In all cases, actual membrane resistances were determined from water flux experiments ($R_M = 1.3 \pm 0.7 \times 10^{12}$ m^{-1} for USD and $2.8 \pm 0.3 \times 10^{12}$ m^{-1} for pilot-scale TFF). Flux rates reported are average values in the steady state region for each of the ΔP_{TMP} studied ($10 < t$ (min) < 15) (where flux values of the mean $\pm$ 5% are achieved) and adjusted by $J_{USD} = \bar{J}(1 - \delta)$ where the factor $(1 - \delta)$ varies from 0.69 to 1.31 for USD and from 0.92 to 1.07 for TFF depending on actual R_M values of each experiment. All trials were run in diafiltration mode (Fig. 1A and B) ($n = 1$). USD runs were performed at 20.0 ± 0.5 °C, while pilot-scale TFF trials occur at room temperature (~20 °C). Feed solutions were mAb-A formulated in 10 mM Tris Acetate at pH 5.4. The diafiltration buffer was 10 mM Tris Acetate at pH 5.4.

experiments at 5 mg/mL (Fig. 4A, i), 15 mg/mL (Fig. 4B, i) and 30 mg/mL (Fig. 4C, i). This allowed the construction of parity plots comparing the USD predicted and the measured pilot-scale TFF flux rates (Fig. 4ii). Good agreement was found particularly at flow conditions >3300 s^{-1} and $\Delta P_{TMP} > 1.0$ bar which is the industrially relevant region for most TFF operations [33]. As indicated from Fig. 4ii the USD system appears to over predict flux at lower shear conditions, lower ΔP_{TMP} values and for lower concentrations. This might be explained by the difference in the nature of flow with the pilot-scale TFF system ($1600 < Re_{USD} < 4600$ versus $2800 < Re_{TFF} < 8500$). Also, using a single ΔP_{TMP} value for the USD studies may not fully capture the conditions and match the average $\Delta\bar{P}_{TMP}$ in the pilot-scale TFF system across the variation of possible localised ΔP_{TMP} along the length of membranes within a cassette. To determine where along the length of the membrane these localised ΔP_{TMP} variations occur and how large these variations are in a pilot-scale TFF system will be a complex undertaking. This could involve designing experiments to study the membrane performance in terms of the permeate flux at different points of a membrane cassette and comparing these with multiple USD trials representing the range of ΔP_{TMP} and flow conditions along the membrane cassette.

3.3. Effect of feed concentration on diafiltration operations

The diafiltration performance of different mAb-B feed concentrations up to 155 mg/mL was evaluated in USD experiments. Due to limited amount of material, only some of the lower feed concentrations, up to 39 mg/mL, were investigated at pilot scale. A crossflow rate, Q_F, of 4.0 LMM was chosen for the TFF system while a disc speed, N, of 2100 rpm for USD trials was selected. These conditions were selected as they have the same shear rates for solution viscosities from 0.00103 Pa·s for 5 mg/mL to 0.00137 Pa· s for 30 mg/mL (Fig. 3iii and 3iv).

The flux was recorded as a function of time during a 7 DV operation in the USD (Fig. 5A, i) and in the pilot-scale TFF systems (Fig. 5B, i). In both systems, steady-state flux was attained for all concentrations, i.e. indicating there was negligible fouling layer resistance ($R_F = 0$). The measured steady-state fluxes for all concentrations studied were plotted in Fig. 5ii and were observed to overlap for both the USD and TFF systems. This further confirms our observation in Section 3.2 that the USD system is able to predict steady-state fluxes achieved by the pilot-scale TFF system at the upper range of transmembrane pressure drops (>1.0 bar) tested. For a given transmembrane pressure, the USD system yielded an exponential-like correlation ($J \propto e^{0.020C}$ ($R^2 = 0.93$)) of the

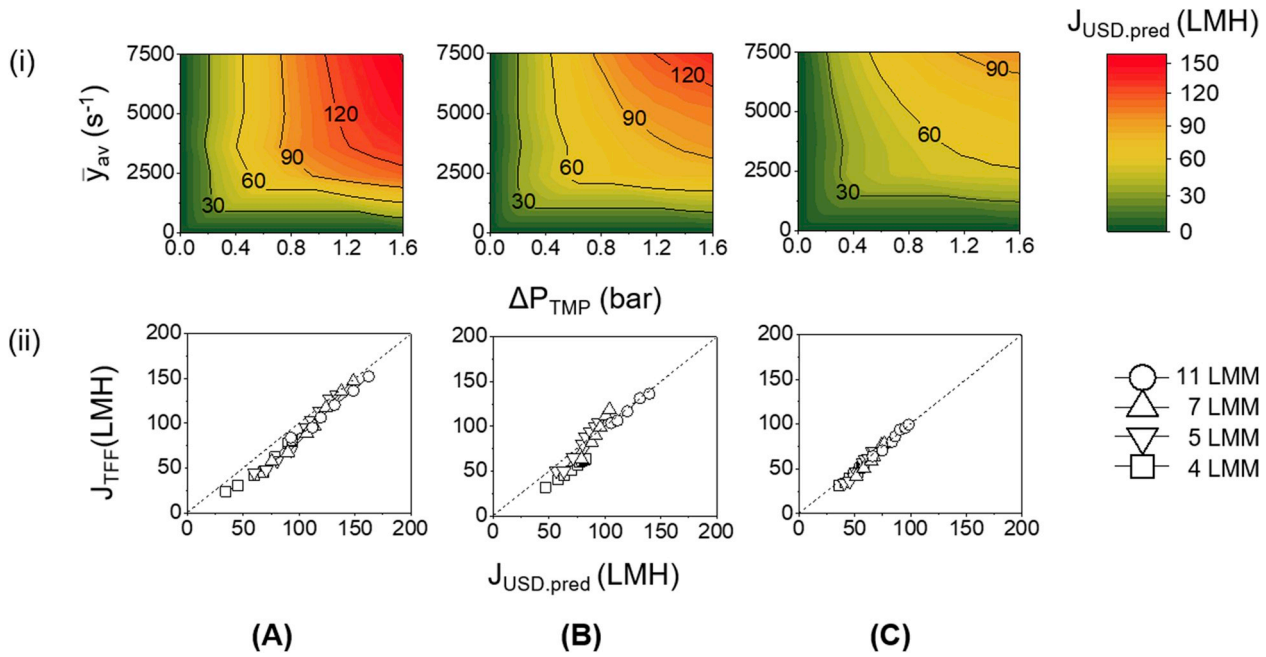

Fig. 4. (i) USD design space predicting flux as a function of average shear rate and transmembrane pressure drop. (ii) Pilot-scale TFF measured flux versus USD predicted flux. The three concentrations of mAb-A used in this study were: (A) 5 mg/mL, (B) 15 mg/mL, and (C) 30 mg/mL). In (i), correlations from Fig. 3i were used to predict values across a design space ($\bar{y}_{av}$: 0 - 7500 s^{-1} and ΔP_{TMP}: 0–1.6 bar). In (ii), the measured flux from the pilot-scale TFF system was obtained from Fig. 3ii. The predicted flux by USD was empirically obtained from (i) at the pilot-scale TFF conditions (Fig. 3iv). The resulting R^2 are: (A) 0.99; (B) 0.98; and (C) 0.99. The diafiltration operations were run as shown in Fig. 1A and B (n = 1).

diafiltration flux with increasing feed concentration. Interestingly, this is similar to the correlation observed between viscosity and concentration in Fig. 2 ($\mu \propto e^{0.017C}$ [31]). The three runs with the previously studied mAb-A achieved similar flux rates (Fig. 3) as for mAb-B as might be expected from their similar rheological properties (Fig. 2).

3.4. Effect of loading/desired retentate concentration in ultrafiltration/diafiltration operations

A fed-batch UF/DF operation was designed by maintaining constant feed/retentate volume over time during both the ultrafiltration and the diafiltration stage in the USD system (Fig. 1C) and the pilot-scale TFF system (Fig. 1D). A single flow condition was tested, i.e. a crossflow rate, Q_F, of 4 LMM for the TFF system. Based on equivalent shear rate at this crossflow rate (Fig. 3iii), a disc speed, N, of 2100 rpm was chosen for the USD trials. The flux was recorded as a function of time in all trials. The four UF/DF experiments used the same initial feed solution of 12 mg/mL. This solution was firstly concentrated using different concentration factors based on different target loadings, and then diafiltered by the same extent of diafiltration (7 DV).

A summary of the loading calculation for all four conditions is included in Table 1. Various mass loadings were initially selected (Table 1 Col 1), which are within the typical range of 200–1000 g/m^2 (the typical loading for protein processing is 450 g/m^2 [4]). The calculated total volumetric loading, volume concentration factor and resulting retentate concentration which corresponds to each of the mass loadings are shown in columns 2, 3 and 4 respectively in Table 1.

During the UF stage, the USD system predicts a decline in flux with increasing desired retentate concentration (Fig. 6i). The pilot-scale TFF system yields similar flux profile and duration as the USD system. As expected, this is a similar decline to that observed in Fig. 5ii. During the DF stage, similar steady-state flux profiles are observed for both scales in all conditions (Fig. 6ii).

The use of the USD system during UF/DF operations gives an insight into the trade-off between the duration and the desired retentate concentrations prior to a diafiltration step. The USD system produces similar UF/DF flux profiles as the pilot-scale TFF system (Fig. 6iii). These results show that the USD system can predict the duration of a UF/DF step at various target mass loadings or final retentate concentrations. The USD flux predictions from these studies may be used to recommend a desired retentate concentration (and therefore, fix a membrane loading) which will meet the overall UF/DF duration requirements of 3–4 h to fit in a regular shift. For example, based on these studies one may recommend a retentate concentration of up to 74 mg/mL if an overall duration of less than 3.5 h is desired (Fig. 6C, iii).

3.5. Comparing product quality between the systems

The final UF/DF step is at the end of a bioprocess, after which only a final bulk filtration for bioburden reduction takes place with no additional purification steps. The main objective of a UF/DF step is to achieve volume reduction (concentrate) and exchange buffer environment (diafilter) while maintaining the product quality, in particular soluble and insoluble aggregation levels. Soluble aggregates can impact potency and safety, while insoluble aggregates could impact the final bulk filtration performance.

3.5.1. Comparing soluble aggregates

The effect of processing on the presence of soluble aggregates, specifically dimers, was determined by the difference in peak areas from a size exclusion chromatogram.

The monomer content of the feed solutions varied from 99.1 ± 0.01% (m = 3) at 0.8 mg/mL (diluted stock), to 98.4 ± 0.04% (m = 3) at 155 mg/mL (stock solution) (*data not shown*) - i.e. a significant change (p = 0.005, *t*-test with alpha level of 0.05). This small difference in monomer content could be due to aggregation being protein concentration dependent and more prone to aggregate-inducing effects such as stirring as observed elsewhere [34,35].

These feed solutions were used for both DF and UF/DF operations. A change in dimer of ±0.5% due to processing was detected across the

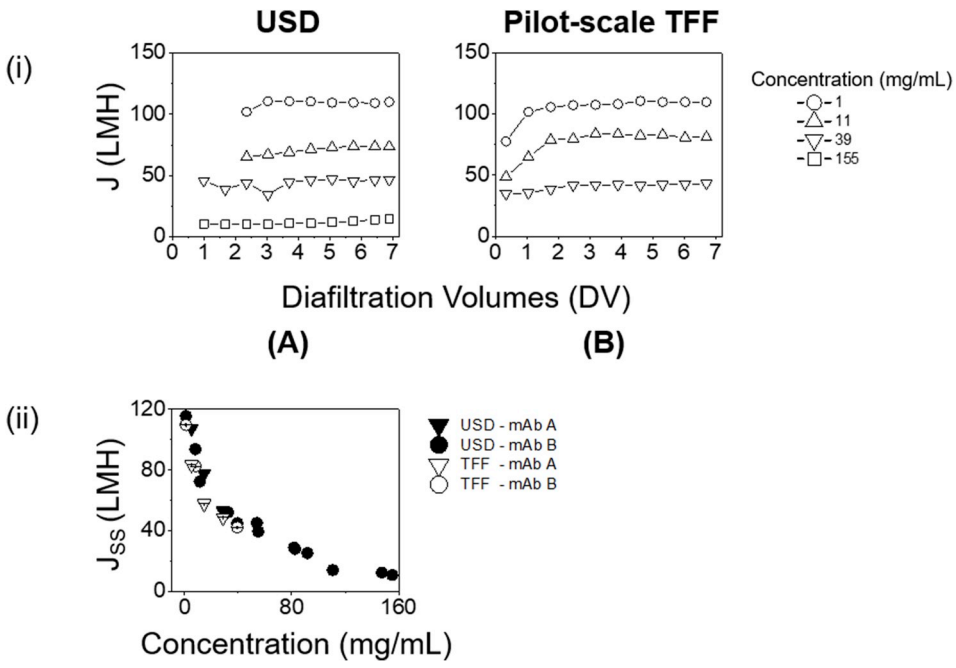

Fig. 5. (i) Effect of feed concentration on the flux as a function of diafiltration volumes for the (A) USD system and (B) pilot-scale TFF system for mAb-B. (ii) Steady-state flux as a function of feed concentration for mAb-A and mAb-B for both systems. In (i) the reported flux values were obtained from moving average of raw data ($m = 100$) where s.d. is ~1%. Due to short experimental durations, the first DV values were not calculated for the lower USD concentrations runs. Twelve additional concentrations between 1 and 155 mg/mL were conducted at the same conditions for the USD system *(data not shown in (i) but the calculated steady fluxes are included in (ii))*. Only three pilot-scale TFF runs were performed at 1, 11 and 39 mg/mL due to limited amount of material. In (ii) the steady-state flux (J_{SS}) was determined from the steady state region ($3.5 < DV < 7.0$) for each run in (i) where flux values of the mean ± 5% are achieved. The error bars lie within the data points and represent the range of the steady-state flux. mAb-A data were obtained from Fig. 3. In all cases, actual membrane resistances were determined from water flux experiments ($R_M = 1.4 \pm 0.5 \times 10^{12}$ m^{-1} for USD and $1.8 \pm 0.3 \times 10^{12}$ m^{-1} for pilot-scale TFF). Flux rates reported are adjusted by multiplying by $(1 - \delta)$ to account for membrane variability as discussed in Ref. [7], which for the mAb-B experiments varied from 0.73 to 1.13 for USD and from 0.99 to 1.05 for TFF. The feed solutions and the diafiltration buffer were made up of 10 mM TrisAcetate at pH 5.4. A constant transmembrane pressure drop, ΔP_{TMP}, of 1.00 ± 0.05 bar was maintained in both systems. All pilot-scale TFF experimental runs were conducted at constant $Q_F = 4$ LMM and the USD trials at constant $N = 2100$ rpm both resulting in equivalent shear rate conditions ($\bar{\gamma}_{av} = 2400$ s^{-1} at 0.00103 Pa·s in Figs. 3 and 4ii). All trials were run in diafiltration mode (Fig. 1A and B) ($n = 1$). Other experimental details are the same as those described in Fig. 3 legend.

range explored in the USD system (Fig. 7i) with a possible decrease with increasing feed concentration. A change in dimer of ±0.25% was measured in the pilot-scale TFF system. These differences are considered to be within the expected level of noise of the system used for these experiments.

3.5.2. *Comparing insoluble aggregates*

An increase in turbidity, measured by OD_{650}, was observed in both systems and attributed to protein colloidal particle formation due to the near absence of non-mAb proteins. Trends of the change in OD_{650} (ΔOD_{650}) as a function of concentration (Fig. 7A, ii) and total experimental duration (Fig. 7B, ii) were obtained for a range of DF and UF/DF trials. The turbidity measurements recorded in the pilot-scale TFF trials were considered to be acceptable for final bulk processing through a 0.22 μm filter during the bioburden reduction stage (private communications, Merck Sharp & Dohme, 2018). At equivalent conditions, ΔOD_{650} values recorded in the USD system were ~50-100 x larger than that for the pilot-scale TFF. This difference was thought to be related to the configuration of each system, discussed later on.

Single-variable experiments were conducted to try and build up a correlation linking turbidity with time, concentration and the different USD and TFF configurations for DF operations, where concentration is fixed. Data from USD studies were used as the starting point in the initial analysis, where it was arbitrarily assumed that the constant $\overline{F}$ is 1 for this system. The retentate OD data, from diafiltration trials conducted in the USD system ($\bar{\gamma}_{av} = 2200$ s^{-1}) with variations in the extent of diafiltration volume *(data not shown)* and feed concentration (Fig. 4), were fitted into a line of best fit resulting in a correlation of $\Delta OD_{650} = 0.0174\ t_{DF}^{0.7} C^{0.996} \overline{F}$ with $R^2 = 0.98$ (Fig. 8A). The exponent values provide some basis in understanding aggregation processes indicating a stronger correlation of the change in OD_{650} with the concentration than with the duration of the diafiltration step. Additional factors such as the extent of diafiltration,

Table 1
Experimental design for ultrafiltration (UF) step in Fig. 6. The mass loading, M_G (Col 1) values were selected by the user. The total volumetric loading, $M_{L.T}$ (Col 2) is another way to define loading and is used to determine total feed volume required in each condition. For example, a $M_{L.T}$ of 17 L/m^2 with $A_{USD} = 0.00021$ m^2 results in a total feed volume, V_T, of 0.003 L. The resulting VCF (Col 3) were determined by $M_{L.T}/M_{L.F/R}$ where $M_{L.F/R} = 8.1$ L/m^2, as fixed with the USD design used in this paper. Desired retentate concentration, C_R (Col 4) is then calculated by C_F·VCF where $C_F = 12$ mg/mL across all conditions.

	(1) Mass loading, M_G (g/m^2)	(2) Total feed volumetric loading, $M_{L.T}$ (L/m^2)	(3) Volume Concentration Factor, VCF (−)	(4) Desired retentate concentration, C_R (mg/mL)
(A)	200	17	2.1	25
(B)	300	25	3.1	37
(C)	600	50	6.2	74
(D)	800	67	8.2	99

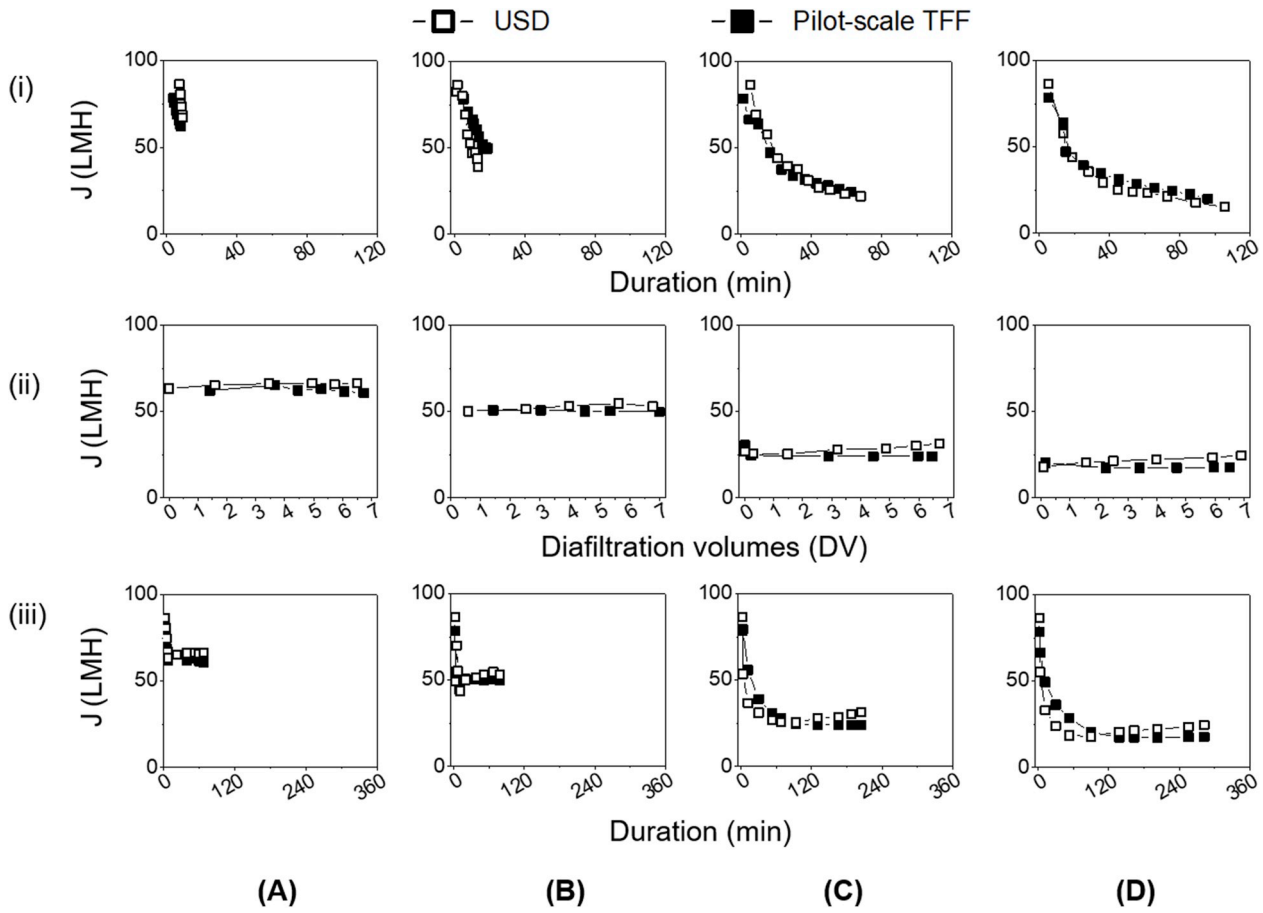

Fig. 6. Effect of the desired retentate concentration on flux profiles for mAb-B during: (i) the UF stage as a function of duration; (ii) the DF stage as a function of diafiltration volumes; and (iii) for the combined UF/DF stages as a function of total duration. The specified mass loadings and the desired retentate concentrations are: (A) 200 g/m^2 ≈ 25 mg/mL, (B) 300 g/m^2 ≈ 37 mg/mL, (C) 600 g/m^2 ≈ 74 mg/mL and (D) 800 g/m^2 ≈ 99 mg/mL (more details provided in Table 1). In all cases, actual membrane resistances were determined from water flux experiments ($R_M = 1.2 \pm 0.2 \times 10^{12}$ m^{-1} for USD and $2.2 \pm 0.3 \times 10^{12}$ m^{-1} for pilot-scale TFF). Flux rates reported are adjusted by a factor $(1 - \delta)$ to account for membrane variability as discussed in Ref. [7], which for these experiments varied from 0.77 to 0.93 for USD and from 1.03 to 1.12 for TFF. An initial feed solution of 12 mg/mL mAb-B in 10 mM Tris Acetate at pH 5.4 was used for all experiments. Other operating conditions are the same as those described in Figs. 3–5 legends.

reversible aggregation and increasing viscosity may also have an impact. In addition, the empirical correlation follows the same first-order correlation with concentration ($\Delta OD_{650} \propto C^1$) found in mAb aggregation studies that investigated the impact of stainless-steel surface in the presence of shear [21,22].

The same trends between ΔOD_{650}, t_{DF} and C were observed for pilot-scale TFF experiments, conducted up to 39 mg/mL, at equivalent membrane flow conditions ($\bar{\gamma}_{av} = 2200$ s^{-1}). The pilot-scale data overlapped with the USD data using a scaling factor $\bar{F} = 0.016$ ($R^2 = 0.99$) (Fig. 8B). This $\bar{F}$ value was obtained from the least sum-of-squares (SS) from the difference between predicted and actual ΔOD_{650}. Further details are described in Fig. 8 legend and Supplementary Table S1.

The same pilot-scale TFF system with an alternative pump type, i.e. rotary lobe, was used at equivalent membrane flow conditions ($\bar{\gamma}_{av} = 2200$ s^{-1}) for similar diafiltration studies. Here a scaling factor of $\bar{F} = 0.068$ was found to fit best in the least-squares linear fit (Fig. 8C). This larger value can be attributed to the larger hold-up volume of the rotary lobe pump head compared with the quaternary diaphragm pump head, i.e. greater high shear zones. The insights regarding what the $\bar{F}$ values obtained for these systems may mean are discussed next alongside additional USD and TFF systems.

More details of these first three experiments are described in Fig. 9: 1.7 mL USD device (Fig. 9, Col 1); a pilot-scale TFF system with diaphragm pump (Fig. 9, Col 2); and a pilot-scale TFF system with rotary lobe pump configuration (Fig. 9, Col 3).

Three additional system configurations were tested. These included: (a) a 6.3 mL USD device (Fig. 9, Col 4) showing greater quiet zone for the same high shear zone than the original 1.7 mL USD device; (b) a variation of the TFF system with decreased start volume (200 mL) in the feed tank for the same pump and membrane cassette (Fig. 9, Col 5); and, (c) a lab-scale TFF system with different tank and membrane configurations, and pump type (Fig. 9, Col 6).

All were conducted in a 7 DV diafiltration operation at equivalent membrane flow conditions. The diafiltration data from these systems were fitted by applying an individual fitted F value with respect to the default USD configuration that resulted in the least sum of squares using the correlation described above.

The following systems described in Fig. 9 have the corresponding $\bar{F}$ (average of fitted F) values in decreasing order: (1) USD system (1.7 mL) > (5) TFF (Quaternary diaphragm pump, 200 mL) > (4) USD system (6.3 mL) > (6) TFF (Millipore TFF® diaphragm pump, 50 mL) > (3) TFF (rotary lobe pump, 890 mL) > (2) TFF (Quaternary diaphragm pump, 890 mL).

The characteristics of each filtration system and their corresponding $\bar{F}$ values were then compared with the assumption that the USD system (1) represents an F value of 1 as the USD data were used as the starting basis for this evaluation (Figs. 8 and 9). The fitted $\bar{F}$ values represent the contribution of the various sources of aggregation within these systems. It is now commonly known that the presence of shear causes aggregation

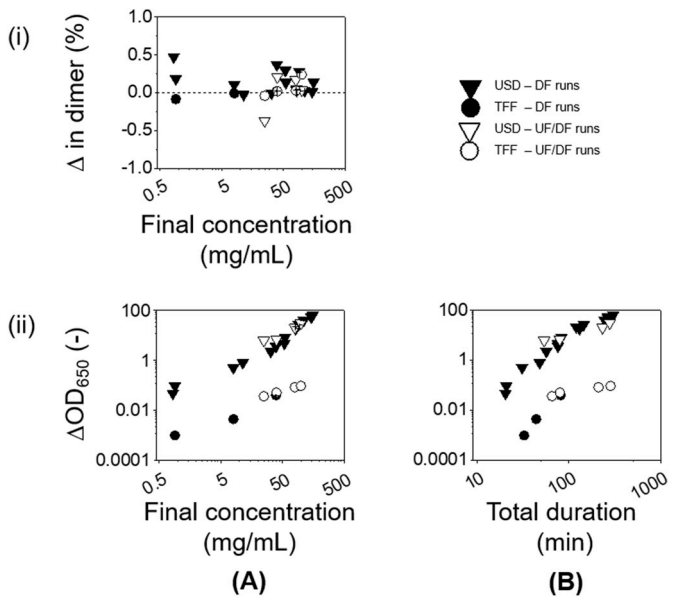

Fig. 7. Effect of the operation and the system used on: (i) the change in dimer and (ii) the change in turbidity due to processing of mAb-B as a function of (A) final (retentate) concentration and (B) total duration of the selected operation. Two operations were studied: DF operations (●, ▼) and UF/DF operations (○, ▽). In (ii) Δ in dimer (%) values are calculated by the difference in dimer present between the feed and the retentate sample at each concentration. In (ii), ΔOD_{650} values are determined by the difference between the OD_{650} value of the retentate and the feed. All feed solutions contained mAb-B formulated in 10 mM Tris Acetate pH 5.4. mAb-A solutions expected to have similar ΔOD_{650} values at equivalent conditions (*data not shown*). All details about the DF-only operations and the UF/DF operations are found in Figs. 5 and 6 legends, respectively.

of proteins [22]. The mechanism of aggregation has also been discussed in detail in other studies (e.g. Ref. [18]). Crucially, these steps involve seeding, nucleation and growth of aggregates. By evaluating the fitted F ($\overline{F}$) values and comparing the characteristics of the different systems, it can be inferred that $\overline{F}$ represents the contribution of the various sources of aggregation within these systems resulting in a change in OD_{650}. Aggregation can be considered to be influenced by three environmental conditions within the systems used in this work: (a) high shear zones promoting aggregation; (b) low shear "quiet" zones where aggregation events cease; and (c) presence of particles that act as "seeds" that initiate aggregate nucleation and growth. The first two conditions could be approximated by the hold-up volumes in each filtration system (Fig. 9). High shear zones (a) are areas near the source of shear in each system, which are the rotating disc in the USD system, and the crossflow pump, membrane cassette and retentate valve in the pilot-scale TFF system. These were identified as those generating shear due to their design and known impact in bioprocessing [22,36]. Quiet zones (b) are defined as the remaining areas in the filtration system not designated as a high shear zone. This includes the volume above the disc for the USD system and the feed/retentate tank for the pilot-scale TFF system. For condition (c), the presence of "seeds" is based on existing literature, for example by Ref. [37], reporting that firstly, stainless steel equipment can potentially shed particles into the solution which can initiate nucleation and aggregate growth and secondly, presence of interfaces, including membrane surface, can induce surface-adsorption leading to aggregation.

These three environmental conditions will be used in the next section to understand the ΔOD_{650} of each system (Fig. 9). The USD system (System 1, $F = 1.00$) has higher ΔOD_{650} than the pilot-scale TFF system (System 2, $\overline{F} = 0.016$, $F_{calc} = 0.053$) due to greater potential of more frequent shear exposure (i.e. lack of quiet zones as a result of the total system hold-up volume being a high shear zone) and increased proximity between the source of shear and active surfaces. In contrast, the modified USD system (4) has a larger quiet zone ($F_{calc} = 0.27$, $\overline{F} = 0.12$) resulting in decreased ΔOD_{650}. This comparison between the fraction of high shear zones over the total system volume (F_{calc}) and the presence of quiet zones also applies when comparing the pilot-scale TFF systems (Systems 2,3,5 and 6) to the USD system.

While $\overline{F}$ is derived from fitting measured and predicted ΔOD_{650}, F_{calc} on the other hand is the ratio of the volume of material exposed to high shear zones to the total system volume. The resultant agreement of $\overline{F}$ and F_{calc} values is reasonable with the latter always being an overestimate. This indicates the need to redefine high shear zones in the various devices if the USD device is to be a more representative predictive tool of the pilot-scale. For example, the fraction of high shear zones may not be the only contributor to the aggregation. The presence of "seeds" and more importantly the combined effect of: "seeds", "high shear zone fraction (F_{calc})" and "seed concentration (dictated by the retentate volume)" may all increase the chances of aggregate formation [22,27,37].

"Seed concentration" may play a role in the observed difference between F_{calc} and $\overline{F}$ in systems with different retentate volume and pumps (i.e. System 3 vs. System 6). The difference between "high shear zone fraction, F_{calc}" and $\overline{F}$ in these two systems could be explained by the

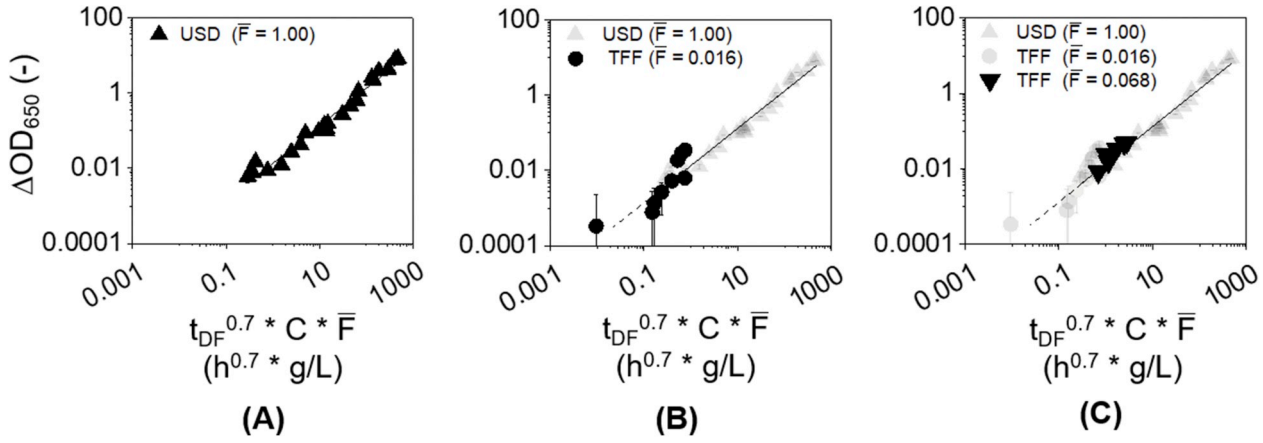

Fig. 8. Effect of diafiltration time, concentration, and fraction of high shear zones on the change in turbidity of mAb-B solutions: (A) USD-only ($\overline{F} = 1.00$, ▲) where $t_{DF} = 0.0–5.1$ h and $C = 1–155$ mg/mL; (B) Pilot-scale TFF system with a quaternary diaphragm pump ($\overline{F} = 0.016$, ●) where $C = 1–39$ mg/mL, $t_{DF} = 0.5–6.8$ h alongside data reproduced from (A); (C) Data from the pilot-scale TFF system with a rotary lobe pump ($\overline{F} = 0.068$,▼), $C = 12$ mg/mL, $t_{DF} = 0.8–7.5$ h. The sample procedure and data acquisition for ΔOD_{650} is described in Fig. 7 legend. The steps used to determine the $\overline{F}$ value using least sum-of-squares method for (B) and (C) are shown in the Supplementary table.

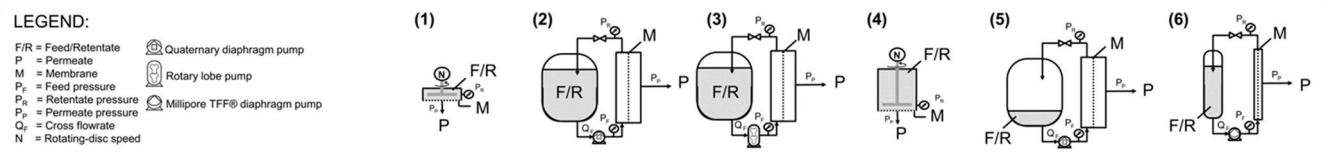

		(1)	(2)	(3)	(4)	(5)	(6)
Volumetric loading (L/m²)		8.1	8.1	8.1	30	1.9	8.1
Area (m²)		0.00021	0.11	0.11	0.00021	0.11	0.005
Feed/Retentate tank volume (L)		0.0017	0.89	0.89	0.0017	0.20	0.041
Quiet zones	Pipework volume (L)	-	0.0059	0.011	-	0.0059	0.0031
	Unsheared feed volume (L)	-	0.89	0.89	0.0046	0.20	0.041
High shear zones	Sheared chamber volume (L)	0.0017	-	-	0.0017	-	-
	Pump type (-)	-	Quaternary Diaphragm	Rotary Lobe	-	Quaternary Diaphragm	Millipore TFF® Diaphragm
	Pump head hold-up volume (L)	-	0.013	0.060	-	0.013	0.00063
	Membrane cassette hold-up volume (L)	-	0.037	0.037	-	0.037	0.0032
	Retentate valve hold-up volume (L)	-	0.000064	0.000064	-	0.000064	-
Total system hold-up volume (L) (= quiet zones + high shear zones)		0.0017	0.95	1.00	0.0063	0.26	0.047
F_{calc} (-) (= sum high shear zones/total system hold-up volume)		1.00	0.053	0.097	0.27	0.19	0.081
$\overline{F}$ (-)		1.00 (Min: 0.41 Max: 2.00)	0.016 (Min: 0.0049 Max: 0.043)	0.068 (Min: 0.047 Max: 0.091)	0.12	0.15	0.077
ΔOD_{650} (-)		0.0061 - 8.4	0.00033 - 0.035	0.0083 – 0.060	0.025	0.032	0.016
Concentration (g/L)		1 - 155	1 - 40	12	12	12	12
Diafiltration time, t_{DF} (h)		0.0 - 5.1	0.5 - 6.8	0.8 - 7.5	1.3	1.3	1.3
Number of diafiltration volumes, DV (-)		0 - 8	4 - 36	4 - 40	2	31	7

Fig. 9. Description of the different USD and pilot-scale TFF system designs. The default configurations are: (1) an ultra scale-down (USD) system with $\overline{F} = 1.00$, and (2) a pilot-scale TFF with $\overline{F} = 0.016$. Set-up (3) explores the type of pump: a modified pilot-scale TFF system (based on 2) with a rotary lobe pump with $\overline{F} = 0.068$. Two set-ups explore the volumetric loading: (4) is a modified USD system (based on 1) with a larger volumetric loading with $\overline{F} = 0.12$ and (5) is a modified pilot-scale TFF system (based on 2) with a smaller volumetric loading with $\overline{F} = 0.15$. Set-up (6) explores an entire different system alongside a new pump; the lab-scale system (Millipore TFF) with a diaphragm pump with $\overline{F} = 0.077$. $\overline{F}$ shown in Fig. 8 refers to systems (1)–(3).

"seed concentration" dominating over F_{calc} when similar F_{calc} systems are compared. System (6) has a smaller retentate volume than in system (3) possibly displaying higher "seed concentration". This can help explain why system (6) has a larger $\overline{F}$ (0.077 vs. 0.068) but a smaller F_{calc} (0.081 vs. 0.097) than system (3). A key assumption here is that the membrane surface has an impact on the creation of "seeds" and is included in the high shear zone area. This assumption is based on the increasingly recognised impact of the interaction of proteins with the membrane surface on aggregate formation [27,37]. Future work would be required to confirm this by conducting control experiments without the presence of a membrane.

An increase in turbidity of the final retentate samples was also observed during UF/DF operations. As with DF-only operations, the USD system consistently showed higher OD changes between initial feed and final retentate samples compared to the pilot-scale TFF *(data not shown)*. The ΔOD_{650} values obtained during UF/DF operation using the USD system follow the same correlation (i.e. $\Delta OD_{650} = 0.0174\ t_{DF}^{\ 0.7}\ C^{0.996}\ \overline{F}$). However, deviations in fitted F values for the pilot-scale TFF system were observed: $\overline{F} = 0.005$ (UF/DF) vs 0.016 (DF-only, shown in Figs. 8B–9). A greater understanding of the turbidity profile with time of the UF/DF steps for both USD and pilot-scale TFF systems is required to analyse the deviations between the two systems.

4. Conclusion

This paper has presented the use of the USD system to predict the membrane performance (i.e. permeate flux) and the product quality (i.e. protein aggregation) of monoclonal antibody diafiltration and ultrafiltration/diafiltration operations. The USD predicted fluxes and the measured fluxes at pilot scale for monoclonal antibody solutions were in good agreement across a range of transmembrane pressures, flow conditions (i.e. average shear rate), and feed concentrations.

A difference in the turbidity of the processed solutions was observed between the USD and pilot-scale TFF system. This was shown to result from differences in the volumes exposed to high-shear stress zones. A correlation between turbidity, time and feed concentration is proposed in this study and fitted across a range of conditions in a total of six systems, two USD and four TFF systems.

Declaration of competing interest

None.

Acknowledgements

The work presented has been funded by: Merck Sharp & Dohme Corp., a subsidiary of Merck & Co., Inc., Kenilworth, NJ, USA; UK Engineering and Physical Sciences Research Council (EPSRC) Centre for Doctoral Training (CDT) in Bioprocess Engineering Leadership (Grant Number: EP/L01520X/1); and Higher Education Funding Council for England (HEFCE) Catalyst Fund. To the best of their knowledge, the authors declare there are no other potential conflicts of interest.

Nomenclature

A	Membrane area (cm^2 or m^2)
C	Solution concentration (mg/mL)
DF	Diafiltration (−)
DV	Diafiltration volumes (−)
F	Individual constant determined by the correlation ($\Delta OD_{650} = 0.0174\ t_{DF}^{0}{}^{.7}\ C^{0.996}\ \overline{F}$) for a single concentration (C), duration (t_{DF}) and ΔOD_{650} (−) for a given system from Fig. 9 (−)
$\overline{F}$	Average of F (only determined when multiple F are available) (−)
F_{calc}	Fraction of high shear rate over system volume (−)
G	Sum of least squares (−)
J	Permeate flux rate ($L/m^2/h$ or LMH)
k	Viscosity constant ($Pa{\cdot}s^n$)
K	Manufacturer's constant (−)
L	Length of cassette (cm)
M	Membrane loading (L/m^2 or g/m^2)
n	Viscosity coefficient (−)
N	Disc speed (rpm)
ΔOD_{650}	Change in optical density at a wavelength of 650 nm (−)
ΔP	Pressure drop across membrane (bar)
P	Fluid pressure (bar)
Q	Flow rate ($L/min/m^2$ of membrane area or LMM)
SS	Least-squares (−)
t	Time (min or h)
UF	Ultrafiltration (−)
UF/DF	Ultrafiltration/diafiltration (−)
VCF	Volume concentration factor (−)
δ	Adjustment factor (−)
ρ	Density ($g\ cm^{-3}$)
μ	Solution dynamic viscosity (Pa·s)
$\bar{y}$	Characteristic shear rate (s^{-1})

Subscripts

av	Average
DF	Diafiltration
F	Feed
L.T	Total volume
L.F/R	Feed/retentate volume
M	Membrane
P	Permeate
R	Retentate
SS	Steady-state
TMP	Transmembrane pressure
W	Water

Appendix A. Supplementary data

Supplementary data to this article can be found online at https://doi.org/10.1016/j.memsci.2019.117606.

References

[1] A.A. Shukla, B. Hubbard, T. Tressel, S. Guhan, D. Low, Downstream processing of monoclonal antibodies — application of platform approaches, Chromatogr. B. 848 (2007) 28–39, https://doi.org/10.1016/j.jchromb.2006.09.026.

[2] B. Kelley, Very large scale monoclonal antibody purification: the case for conventional, Biotechnol. Prog. 23 (2007) 995–1008.

[3] J. Curling, The development of antibody purification technologies. Process Scale Purif. Antibodies, second ed., John Wiley & Sons, Ltd, London, UK, 2009, pp. 25–51, https://doi.org/10.1007/SpringerReference_84249.

[4] H. Lutz, Ultrafiltration for Bioprocessing, first ed., Woodhead Publishing, Elsevier, Cambridge, UK, 2015.

[5] R. van Reis, E.M. Goodrich, C.L. Yson, L.N. Frautschy, S. Dzengeleski, H. Lutz, Linear scale ultrafiltration, Biotechnol. Bioeng. 55 (1997) 737–746, https://doi.org/10.1002/(SICI)1097-0290(19970905)55:5<737:AID-BIT4>3.0.CO;2-C.

[6] M. Dosmar, F. Meyeroltmanns, M. Gohs, Factors influencing ultrafiltration scale-up, Bioprocess Int. 3 (2005) 40–50.

[7] L. Fernandez-Cerezo, A.C.M.E. Rayat, A. Chatel, J.M. Pollard, G.J. Lye, M. Hoare, An ultra scale-down method to investigate monoclonal antibody processing during tangential flow filtration using ultrafiltration membranes, Biotechnol. Bioeng. 116 (2019) 581–590, https://doi.org/10.1002/bit.26859.

[8] H.F. Liu, J. Ma, C. Winter, R. Bayer, Recovery and purification process development for monoclonal antibody production, mAbs 2 (2010) 480–499, https://doi.org/10.4161/mabs.2.5.12645.

[9] P. Rajniak, S.C. Tsinontides, D. Pham, W.A. Hunke, S.D. Reynolds, R.T. Chern, Sterilizing filtration-Principles and practice for successful scale-up to manufacturing, J. Membr. Sci. 325 (2008) 223–237, https://doi.org/10.1016/j.memsci.2008.07.049.

[10] R.V. Cordoba-Rodriguez, Aggregates in mAbs and recombinant therapeutic proteins: a regulatory perspective, Biopharm. Int. 21 (2008) 44–53, doi:(11):44-53.

[11] J.S. Philo, Is any measurement method optimal for all aggregate sizes and types? Am. Assoc. Pharm. Sci. 8 (2006) 564–571, https://doi.org/10.1208/aapsj080365.

[12] M.E.M. Cromwell, E. Hilario, F. Jacobson, Protein aggregation and bioprocessing, Am. Assoc. Pharm. Sci. 8 (2006) 572–579, https://doi.org/10.1208/aapsj080366.

[13] J. Patel, R. Kothari, R. Tunga, N.M. Ritter, B.S. Tunga, Stability considerations for biopharmaceuticals, Part 1: overview of protein and peptide degradation pathways, Bioprocess Int. 9 (2011) 20–31.

[14] A. Mitraki, J. King, Protein folding intermediates and inclusion body formation, Allian Protein Lab. 1 (1989) 690–697, https://doi.org/10.1038/nbt0789-690.

[15] A.L. Fink, Protein aggregation: folding aggregates, inclusion bodies and amyloid, Fold. Des. 3 (1998) 9–23, https://doi.org/10.1016/S1359-0278(98)00002-9.
[16] J.D. Andya, C.C. Hsu, S.J. Shire, Mechanisms of aggregate formation and carbohydrate excipient stabilization of lyophilized humanized monoclonal antibody formulations, Am. Assoc. Pharm. Sci. 5 (2003) 21–31, https://doi.org/10.1208/ps050210.
[17] F. Plath, P. Ringler, A. Graff-Meyer, H. Stahlberg, M.E. Lauer, A.C. Rufer, M. A. Graewert, D. Svergun, G. Gellermann, C. Finkler, J.O. Stracke, A. Koulov, V. Schnaible, Characterization of mAb dimers reveals predominant dimer forms common in therapeutic mAbs, mAbs 8 (2016) 928–940, https://doi.org/10.1080/19420862.2016.1168960.
[18] J.S. Philo, T. Arakawa, Mechanisms of protein aggregation, Curr. Pharmaceut. Biotechnol. 10 (2009) 348–351, https://doi.org/10.2741/e781.
[19] D.W. Knutson, A. Kijlstra, H. Lentz, L.A. van Es, Isolation of stable aggregates of igg by zonal ultracentrifugation in sucrose gradients containing albumin, Immunol. Investig. 8 (1979) 337–345, https://doi.org/10.3109/08820137909050047.
[20] T.J. Narendranathan, P. Dunnill, The effect of shear on globular proteins during ultrafiltration: studies of alcohol dehydrogenase, Biotechnol. Bioeng. (1982), https://doi.org/10.1002/bit.260240917.
[21] J. Bee, J.L. Stevenson, B. Mehta, J. Svitel, J. Pollastrini, R. Platz, E. Freund, J. F. Carpenter, T.W. Randolph, Response of a concentrated monoclonal antibody formulation to high shear, Biotechnol. Bioeng. 103 (2009) 936–943, https://doi.org/10.1002/bit.22336.
[22] J. Biddlecombe, A. Craig, H. Zhang, S. Uddin, S. Mulot, B. Fish, D. Bracewell, Determining antibody stability: creation of solid-liquid interfacial effects within a high shear environment, Biotechnol. Prog. 23 (2007) 1218–1222, https://doi.org/10.1021/bp0701261.
[23] R. Tavakoli-Keshe, J.J. Phillips, R. Turner, D.G. Bracewell, Understanding the relationship between biotherapeutic protein stability and solid-liquid interfacial shear in constant region mutants of IgG1 and IgG4, J. Pharm. Sci. 103 (2014) 437–444, https://doi.org/10.1002/jps.23822.
[24] R. van Reis, A.L. Zydney, Bioprocess membrane technology, J. Membr. Sci. 297 (2007) 16–50, https://doi.org/10.1016/j.memsci.2007.02.045.
[25] T. Kiefhaber, R. Rudolph, H.H. Kohler, J. Buchner, Protein aggregation in vitro and in vivo: a quantitative model of the kinetic competition between folding and aggregation, Nat. Biotechnol. 9 (1991) 825–829, https://doi.org/10.1038/nbt0991-825.
[26] A. Bódalo, J.L. Gómez, E. Gómez, M.F. Máximo, M.C. Montiel, Study of L-aminoacylase deactivation in an ultrafiltration membrane reactor, Enzym. Microb. Technol. 35 (2004) 261–266, https://doi.org/10.1016/j.enzmictec.2004.05.003.
[27] A. Arunkumar, N. Singh, E.G. Schutsky, M. Peck, R.K. Swanson, M.C. Borys, Z.J. Li, Effect of channel-induced shear on biologics during ultrafiltration/diafiltration (UF/DF), J. Membr. Sci. 514 (2016) 671–683, https://doi.org/10.1016/J.MEMSCI.2016.05.031.
[28] A.S. Chandavarkar, Dynamics of Fouling of Microporous Membranes by Proteins, PhD Thesis. Massachusetts Institute of Technology, 1990. https://dspace.mit.edu/handle/1721.1/13642. (Accessed 15 June 2018).
[29] M. Meireles, P. Aimar, V. Sanchez, Albumin denaturation during ultrafiltration: effects of operating conditions and consequences on membrane fouling, Biotechnol. Bioeng. 38 (1991) 528–534, https://doi.org/10.1002/bit.260380511.
[30] M. Vázquez-Rey, D. Lang, Aggregates in monoclonal antibody manufacturing processes, Biotechnol. Bioeng. 108 (2011) 1494–1508, https://doi.org/10.1002/bit.23155.
[31] W.G. Lilyestrom, S. Yadav, S.J. Shire, T.M. Scherer, Monoclonal antibody self-association, cluster formation, and rheology at high concentrations, J. Phys. Chem. B 117 (2013) 6373–6384, https://doi.org/10.1021/jp4008152.
[32] J.F. Richardson, J.M. Coulson, Liquid filtration, in: Chem. Eng, fifth ed., Elsevier, Oxford, UK, 2002, pp. 372–386, https://doi.org/10.1201/b11072-8.
[33] E. Rosenberg, S. Hepbildikler, W. Kuhne, G. Winter, Ultrafiltration concentration of monoclonal antibody solutions: development of an optimized method minimizing aggregation, J. Membr. Sci. 342 (2009) 50–59.
[34] C.R. Thomas, D. Geer, Effects of shear on proteins in solution, Biotechnol. Lett. 33 (2011) 443–456, https://doi.org/10.1007/s10529-010-0469-4.
[35] O. Santos, T. Nylander, M. Paulsson, C. Trägårdh, Whey protein adsorption onto steel surfaces - effect of temperature, flow rate, residence time and aggregation, Food Eng. 74 (2006) 468–483, https://doi.org/10.1016/j.jfoodeng.2005.03.037.
[36] A.C.M.E. Rayat, G.J. Lye, M. Micheletti, A novel microscale crossflow device for the rapid evaluation of microfiltration processes, J. Membr. Sci. 452 (2014) 284–293, https://doi.org/10.1016/j.memsci.2013.10.046.
[37] J.S. Bee, T.W. Randolph, J.F. Carpenter, S.M. Bishop, M.N. Dimitrova, Effects of surfaces and leachables on the stability of biopharmaceuticals, J. Pharm. Sci. 100 (2011) 4158–4170, https://doi.org/10.1002/jps.